Laboratory measurements and theoretical modeling of seismoelectric interface response and coseismic wave fields

M. D. Schakel,[1,a)] D. M. J. Smeulders,[1,2,b)] E. C. Slob,[1,c)] and H. K. J. Heller[1,d)]
[1]*Department of Geotechnology, Delft University of Technology, PO Box 5048, 2600 GA, Delft, The Netherlands*
[2]*Department of Mechanical Engineering, Eindhoven University of Technology, PO Box 513, 5600 MB, Eindhoven, The Netherlands*

(Received 28 October 2010; accepted 18 February 2011; published online 5 April 2011; publisher error corrected 8 April 2011)

A full-waveform seismoelectric numerical model incorporating the directivity pattern of a pressure source is developed. This model provides predictions of coseismic electric fields and the electromagnetic waves that originate from a fluid/porous-medium interface. An experimental setup in which coseismic electric fields and interface responses are measured is constructed. The seismoelectric origin of the signals is confirmed. The numerically predicted polarity reversal of the interfacial signal and seismoelectric effects due to multiple scattering are detected in the measurements. Both the simulated coseismic electric fields and the electromagnetic waves originating from interfaces agree with the measurements in terms of travel times, waveform, polarity, amplitude, and spatial amplitude decay, demonstrating that seismoelectric effects are comprehensively described by theory. © *2011 American Institute of Physics*. [doi:10.1063/1.3567945]

I. INTRODUCTION

Grain surfaces in contact with an electrolyte acquire a chemically bound surface charge that is balanced by mobile counter ions in a thin fluid layer surrounding the grains. The distribution of the mobile ions is determined by a balance between the electrostatic forces and thermal diffusivity. At the interface between the immobile and counter ions the so-called zeta-potential is defined. This electric potential decreases exponentially when one moves away from the interface. The characteristic decay length (the Debye length) is on the order of a few nanometers for typical grain-electrolyte combinations.[1] The ensemble of bound and mobile charge layers is referred to as the electric double layer.

When the pore fluid is in motion, the mobile counter ions in the double layer are transported by the flow with respect to the charge bound to the grain surface. Thus a seismic wave that travels through a porous medium generates an electric wave current on the scale of the wavelength. A comprehensive theory for coupled seismic and electromagnetic wave propagation identifying the zeta-potential as the key parameter was derived by Pride.[1] Two seismoelectric effects can be distinguished: (1) a coseismic electric field is confined to seismic waves and therefore propagates with seismic wave velocity[2] and (2) a seismic wave that traverses a boundary between two distinct porous media produces electromagnetic (EM)-waves that propagate outside the support of the seismic waves with much higher EM-wave speeds.[2,3] Following the terminology in Ref. 4 we refer to the latter as the interface response. Both coseismic and interface response effects are visible in full-waveform numerical simulations.[3–7] Furthermore, a wide range of field and laboratory validations of the coseismic field and the interface response was presented in the literature.[8–21] Several of these works compare either field measurements[15,17] or laboratory measurements[20] with a seismoelectric wave propagation model, corroborating that the coseismic and interface response fields are predicted by the theory.

In this article we complement the study presented in Ref. 20 by developing a full waveform seismoelectric model for the coseismic and interface response fields based on the Sommerfeld integral, and comparing the numerical predictions with laboratory measurements. We demonstrate the seismoelectric nature of the measured electric potentials in a control experiment. The results are distinct from previous studies in the sense that measured seismoelectric multiples as well as a polarity reversal across an interface are predicted by our model and a typical directivity pattern of the acoustic source wavefield is incorporated in the simulation.

II. MODELING OF COSEISMIC AND INTERFACE RESPONSE FIELDS

We describe our modeling approach in the context of numerical simulations of our laboratory experiments. An isotropic homogeneous fluid-saturated porous medium layer is within a compressible fluid (see Fig. 1). The acoustic source pressure is modeled as a modified spherical wave source[22]

$$\hat{p}(\omega, R, \theta) = \frac{A(\omega)\, D(\theta)}{R} \exp[-ikR], \qquad (1)$$

[a)]Author to whom correspondence should be addressed. Electronic mail: M.D.Schakel@tudelft.nl.
[b)]Electronic mail: D.M.J.Smeulders@tue.nl.
[c)]Electronic mail: E.C.Slob@tudelft.nl.
[d)]Electronic mail: H.K.J.Heller@tudelft.nl.

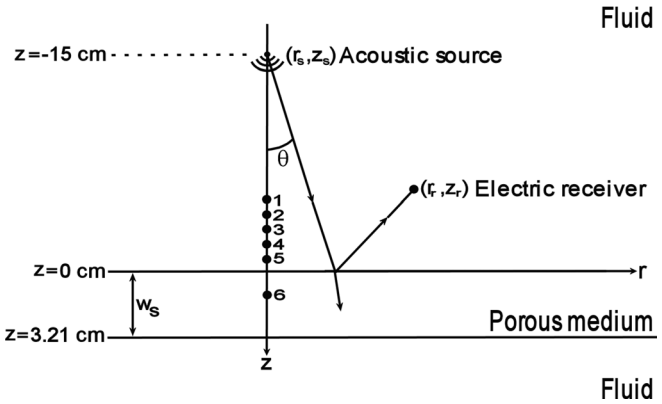

FIG. 1. Geometry of the seismoelectric model and measurements. The total electric potential wavefield is given by an integral over complex-valued θ [Eqs. (5) and (8)]. Positions 1–5 are separated by 0.5 cm with position 1 at $(r, z) = (0, -2.3)$ cm and position 5 at $(r, z) = (0, -0.3)$ cm. Position 6 is at $(r, z) = (0, 1)$ cm.

where ω is the radial frequency, $R = \sqrt{(r - r_s)^2 + (z - z_s)^2}$ is the distance to the source, θ the angle of incidence, $A(\omega)$ is the amplitude spectrum and k is the fluid wavenumber. The directivity function $D(\theta)$, that characterizes the radiation pattern of the source, is given by:

$$D(\theta) = \frac{J_1(ka \sin\theta)}{ka \sin\theta}. \tag{2}$$

Here, J_1 is the Bessel function of the first kind and first order and a is the radius of the transducer. The modeled source pressure wavefield is expanded into conical waves by means of the Sommerfeld integral.[23,24] The total reflected electric potential in the fluid $\hat{\varphi}(\omega, r_r, z_r)$, received at position (r_r, z_r), can then be expressed as $(r_s = 0; z_s, z_r < 0)$:

$$\hat{\varphi}(\omega, r_r, z_r) = -iA(\omega) \int_0^\infty \frac{k_r}{k_z} D(k_r) J_0(k_r r_r) \exp[ik_z z_s] \times R^E(k_r) \exp\left[ik_z^E z_r\right] dk_r, \tag{3}$$

where $k_r = k \sin\theta$ and $k_z = k \cos\theta$ are the radial and vertical components of k, respectively, and k_z^E is the vertical component of the fluid EM wavenumber. The seismoelectric conversion coefficient, $R^E(k_r)$, relates the incident pressure wavefront to an EM signal in the fluid. This conversion coefficient was derived in Ref. 25 adopting full seismoelectric theory. Note that this coefficient is distinct from an ordinary reflection coefficient as it describes the conversion of mechanical energy into EM energy. Also note that the notation in Ref. 25 is slightly different (see Table I). Expressing k_r and k_z in terms of k and θ, Eq. (3) is written as,

TABLE I. Relation between seismoelectric conversion coefficients in this paper and those given in Ref. 25. The fluid density is denoted by ρ_f.

This paper	Reference 25
R^E	$R^E/\rho_f\omega^2$
T_f^{TM}	$\alpha^{TM}T^{TM}/\rho_f\omega^2$
αT_f^{Pf}	$\alpha^{Pf}T^{Pf}/\rho_f\omega^2$

$$\hat{\varphi}(\omega, r_r, z_r) = -iA(\omega) \int_0^{\pi/2+i\infty} D(\theta)\, k \sin\theta J_0(kr_r \sin\theta) \times \exp[ikz_s \cos\theta] R^E(\theta) \exp\left[ik_z^E(\theta) z_r\right] d\theta, \tag{4}$$

where $k_z^E(\theta) = \omega\sqrt{1/c_E^2(\omega) - \sin^2\theta/c_P^2}$ and $\mathrm{Im}\left[k_z^E(\theta) < 0\right]$, with $c_E(\omega)$ and c_P the fluid EM and pressure wave velocities, respectively. The path of integration is along straight lines from 0 to $\pi/2$ and from $\pi/2$ to $\pi/2 + i\infty$ in the complex θ-plane. The second integral over complex θ is simplified further by employing the substitution $\theta = \pi/2 + i\ln\left[\sqrt{\gamma^2 + 1} + \gamma\right]$:

$$\hat{\varphi}(\omega, r_r, z_r) = -\frac{iA(\omega)}{a} \int_0^{\pi/2} J_0(kr_r \sin\theta) J_1(ka \sin\theta) \times \exp[ikz_s \cos\theta] R^E(\theta) \exp\left[ik_z^E(\theta) z_r\right] d\theta + \frac{A(\omega)}{a} \int_0^\infty J_0\left(kr_r\sqrt{\gamma^2 + 1}\right) \frac{J_1\left(ka\sqrt{\gamma^2 + 1}\right)}{\sqrt{\gamma^2 + 1}} \times \exp[kz_s \gamma] R^E(\gamma) \exp\left[ik_z^E(\gamma) z_r\right] d\gamma, \tag{5}$$

where Eq. (2) was used for $D(\theta)$. Equation (5) can readily be numerically evaluated and yields the total reflected EM wavefield in the fluid.

In the porous medium, pressure waves propagate accompanied by their coseismic fields. We take into account the coseismic field belonging to the pressure wave transmitted from the fluid to the porous medium, and the one belonging to the pressure wave that is subsequently reflected from the back of the sample. Only the (fast) pressure (Pf)-wave is considered as it carries virtually all of the acoustic energy. The acoustic waves generate freely propagating transverse magnetic (TM) EM-waves when they encounter interfaces. We take three subsequently generated interface responses into account. We incorporate these coseismic and interface response fields into the Sommerfeld integral. Analogously to Eq. (3) we arrive at the following expression for the electric potential within the porous medium $(r_s = 0;\ z_s < 0$ and $z_r > 0)$,

$$\hat{\varphi} = -iA \int_0^\infty \frac{k_r}{k_z} D J_0 \exp[ik_z z_s] \left\{ T_f^{TM} \exp\left[-ik_z^{TM} z_r\right] + T_f^{Pf} \left[\alpha \exp\left(-ik_z^{Pf} z_r\right) + \exp\left(-ik_z^{Pf} w_s\right) S^E\right] \right\} dk_r, \tag{6}$$

where the functional dependencies are not explicitly written. The width of the porous sample is denoted as w_s. The term $T_f^{TM}\exp\left[-ik_z^{TM} z_r\right]$ describes the propagation of the first TM-wave to the receiver at z_r. This wave is generated at $z = 0$ by the incident acoustic wave from the fluid. T_f^{TM} represents the transmission of converted electric potential due to incident acoustic potential at the front of the sample. The term $\alpha T_f^{Pf}\exp\left[-ik_z^{Pf} z_r\right]$ describes the coseismic electric field traveling along with the Pf-wave in the porous medium. The amplitude ratio between the electric and the pressure fields is described by α, and T_f^{Pf} is the acoustic transmission coefficient. The Pf-wave travels to the back of the porous sample where it is reflected upward. The associated seismoelectric effects are described by S^E,

$$S^E = R_b^{TM}\exp\left[-ik_z^{TM}(w_s - z_r)\right] + R_b^{Pf}\left\{\alpha\exp\left[-ik_z^{Pf}(w_s - z_r)\right] + \exp\left[-ik_z^{Pf}w_s\right]R_f^{TM}\exp\left[-ik_z^{TM}z_r\right]\right\}. \quad (7)$$

The first two terms in Eq. (7) describe the upwardly propagating second TM and coseismic waves, respectively. The last term describes the third interface response that is generated at $z=0$ by the incident Pf-wave from below and now propagates downward as a TM-wave to the receiver. The seismoelectric conversion coefficients at the back and the front of the sample are denoted as R_b^{TM} and R_f^{TM}, respectively. The reflection coefficient for the Pf-wave at the back of the sample is denoted R_b^{Pf}. These coefficients at a fluid/porous-medium interface due to an incident Pf-wave are derived in a procedure similar to the one described in Ref. 25. The notations are slightly different from those in Ref. 25 (see Table I). In a similar way as for Eq. (5), we find from Eq. (6):

$$\hat{\varphi} = -\frac{iA}{a}\int_0^{\pi/2} J_0 J_1 \exp[ikz_s\cos\theta] \times\left\{T_f^{TM}\exp\left[-ik_z^{TM}z_r\right] + T_f^{Pf}\left[\alpha\exp\left(-ik_z^{Pf}z_r\right) + \exp\left(-ik_z^{Pf}w_s\right)S^E\right]\right\}d\theta + \frac{A}{a}\int_0^{\infty} J_0\frac{J_1}{\sqrt{\gamma^2+1}}\exp[kz_s\gamma] \times\left\{T_f^{TM}\exp\left[-ik_z^{TM}z_r\right] + T_f^{Pf}\left[\alpha\exp\left(-ik_z^{Pf}z_r\right) + \exp\left(-ik_z^{Pf}w_s\right)S^E\right]\right\}d\gamma, \quad (8)$$

TABLE II. Parameters of the porous medium. The temperature is 293.15 K.

Bulk modulus skeleton grains[a]	49.9×10^9	Pa
Bulk modulus (pore) fluid[b]	2.2×10^9	Pa
Pore fluid viscosity[b]	1×10^{-3}	Pa s
(pore) Fluid density[b]	998	kg/m^3
Relative permittivity of the (pore) fluid[b]	80.1	—
Relative permittivity of the solid[b]	4	—
(fluid) Magnetic permeability ($=\mu_0$)	$4\pi\times10^{-7}$	H/m
Weighted pore volume-to-surface ratio[c]	9.43×10^{-6}	m
Bulk modulus framework of grains[d]	0.93×10^9	Pa
Shear modulus framework of grains[d]	0.88×10^9	Pa
Porosity of the porous medium[d]	0.52	—
Solid density[d]	2570	kg/m^3
Permeability[d]	3.4×10^{-12}	m^2
Tortuosity[d]	1.7	—
(pore) Fluid conductivity[e]	4.8×10^{-2}	S/m
Zeta-potential[f]	-4×10^{-2}	V
Sample width[e]	3.21×10^{-2}	m

[a]Reference 26.
[b]Reference 27. We take the value of Pyrex 7070 glass for the solid permittivity.
[c]References 1, 28–30.
[d]See N5B in Ref. 31.
[e]Measured values.
[f]See Ref. 32. We assume that conductivity is due to a NaCl salt solution and pH = 6.

where Eq. (2) was used for $D(\theta)$. Equation (8) describes the electric potential within the porous medium. Equations (5) and (8) are numerically evaluated through the inverse fast Fourier transform. For each frequency we use a recursive adaptive Simpson quadrature algorithm implemented in MATLAB. An experimentally recorded pressure waveform at $(r, z) = (0, 0)$ is used for $A(\omega)$ and a 144–896 kHz numerical band-pass filter is applied. The input parameters of Table II are used. Figure 2 (left) shows the resulting modeled reflected electric potentials at positions 1–6 along the z-axis (Fig. 1).

An electric pulse is computed around 0.10 ms at each position, which corresponds to the travel time of the acoustic wave from the source to the porous medium surface, where it generates an EM signal. Due to the large fluid EM-wave speed ($\sim1.0\times10^7$ m/s), the electric pulses arrive almost simultaneously at each position. Note that the pulse decays in amplitude as the distance from the interface increases (positions 1–5 in Fig. 1). Position 6 is inside the porous medium. The first pulse arriving around 0.10 ms at this position has a reversed polarity with respect to the fluid computations. This observation is in agreement with the description of the interface response modeled as the radiation from an oscillating electric dipole oriented vertically with respect to the interface.[3,15] The second pulse at position 6 arrives 5.7 μs later. It travels along with the Pf-wave at

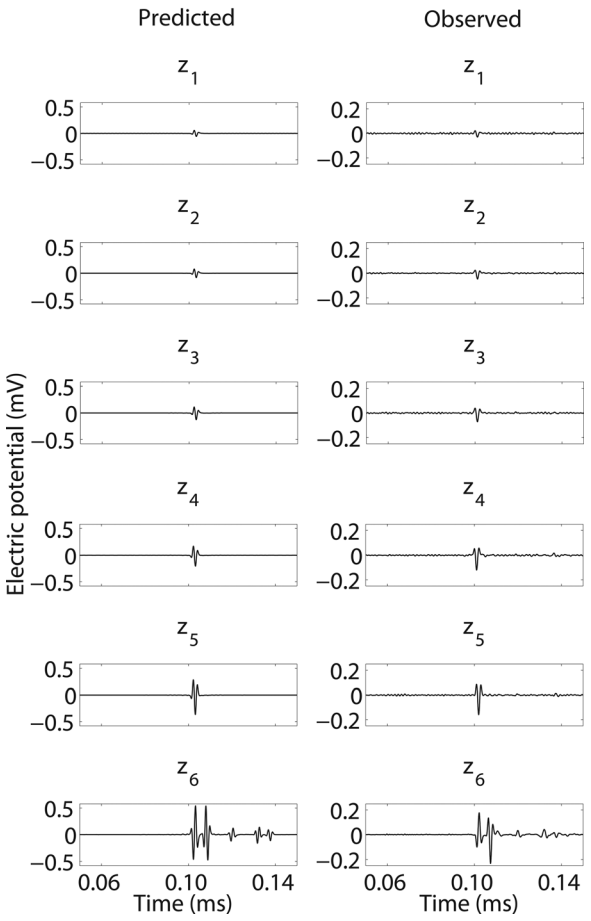

FIG. 2. Numerical electric potential waveform predictions (left) and measurements (right) within the fluid (positions 1–5) and within the porous sample (position 6).

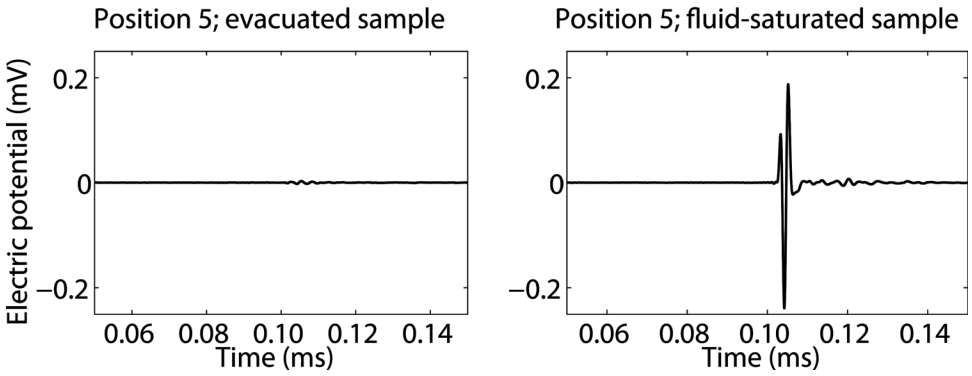

FIG. 3. Electric potential measurement at position 5 on evacuated (left) and fluid- saturated (right) porous sample.

approximately 1900 m/s from the front of the sample to position 6. Therefore it is due to the coseismic electric field supported by the Pf-wave. The pulse arriving around 0.12 ms corresponds with the Pf-wave travel time to the back of the porous sample, where it generates a reflected EM-wave. The fourth and fifth pulses are, respectively, coseismic and interface responses of the compressional wave multiple.

III. SEISMOELECTRIC EXPERIMENTS

A. Seismoelectric experimental setup and measurements

The experimental setup consists of a $58 \times 39 \times 28$ cm water tank in which an acoustic wave source transducer (Panametrics V3638), grounded electrodes (A-M Systems, Inc., Ag/AgCl diameter 0.015 in.), and a porous sample are installed. The geometry of the experiment is depicted in Fig. 1. The sample is made of sintered crushed glass (parameters listed in Table II), carefully saturated, and immersed in tap water. The electrode at position 6 is installed in a 1.4 mm diameter cylindrical hole, which was drilled in the porous sample. A 500 kHz single sine pulse (with a 500 mV peak-to-peak amplitude) from a waveform generator (Agilent Technologies 33220A) is fed into an amplifier (ENI 2100L RF Power Amplifier) set at 50 dB gain. The output signal is coupled into a piezoelectric source transducer. A 144–896 kHz band-pass filter is applied in all measurements. Electric potential measurements were performed at positions 1–6. These on-axis measurements are averaged over 8192 source pulses and shown in Fig. 2 (right). Indeed, the measured seismoelectric pulse patterns are predicted by the model.

The predicted electric potentials (Fig. 2, left) agree with the measurements (Fig. 2, right) in terms of travel times, waveform, polarity, and the spatial amplitude decay. Note that the panels on the right are scaled down by a factor of 2.5. This means that the measured amplitudes are lower than predicted, which can be explained by uncertainties in the parameters given in Table II. Notably, our assumption on the zeta-potential may not be fully appropriate. Identical amplitude scaling is present in all the reflected interface response signals at positions 1–5 and the transmitted signal at position 6 that contains coseismic and interface response effects. This means that, by introducing a scaling factor, all coseismic and interface response effects are correctly described by theory. The small remaining differences in waveform are probably related to minor geometric misalignment in the experiments (the transducer-porous sample-electrode geometry deviates slightly from the model geometry) and to the ruggedness of the porous sample surface. Also, the predicted polarity reversal across the fluid/porous-medium interface (positions 1–5 versus position 6) is clearly visible in the measurements. In Ref. 13 a polarity reversal was also reported in a borehole penetrating the water table. Faint arrivals after the first interface response signal are observed in the recordings at positions 4–5. These do not appear in the computed signals, because only the first interface response is modeled for the fluid positions.

B. Seismoelectric control experiment

We also performed a control experiment to identify seismoelectric conversion as the single mechanism for the electric potential generation. A sample was dried and jacketed before it was immersed in water. A vacuum pump continuously evacuated the sample. Figure 3 (left) shows the measurement at position 5. No appreciable signal can be detected by the electric receiver. Subsequently, the jacketed sample was carefully saturated with de-ionized water and the seismoelectric experiment was repeated. Figure 3 (right) shows the result. Now a clear pulse arrives around 0.10 ms. This experiment unambiguously identifies seismoelectric conversion as the mechanism for electric signal generation. In Refs. 10 and 20 similar conclusions are drawn from different seismoelectric experiments. It is well-known that solids may generate electric effects when under strain, which is referred to as piezoelectricity. This effect however, cannot explain the observations in Fig. 3, as any piezoelectricity would be screened by the electrolyte.[2]

IV. CONCLUSIONS

A seismoelectric numerical model incorporating a typical directivity pattern of the acoustic source wavefield provided full-waveform numerical predictions for both the coseismic and interface response effects. The existence of the seismoelectric coupling phenomenon was validated in our experimental setup. Measurements of the coseismic electric field and the fluid/porous-medium interface response were performed. Agreement between the predicted and

measured wavefields was shown in terms of travel times, waveform, polarity, and the spatial amplitude decay. Furthermore, the predicted polarity reversal and Pf-wave multiple scattering effects were validated by the measurements. The unresolved scaling issue is probably primarily caused by variations in pore fluid conductivity and the zeta-potential that are inaccessible to direct independent measurements. Yet, the overall agreement between the measurements and numerical predictions convincingly validates the existing seismoelectric theory. As both the numerical and experimental techniques can be generalized to field situations, this work allows us to appreciate the use of seismoelectric effects as exploration techniques that are complementary to conventional seismic surveys for exploring the subsurface.

ACKNOWLEDGMENTS

This research was funded as a Shell-FOM (Fundamental Research on Matter) project within the research program "The physics of fluids and sound propagation." The technical support of Jolanda van Haagen is greatly appreciated. M.D.S. also thanks Zhenya Zhu, Gabriel Chao, Bobby Hak, Christiaan Schoemaker, and Karel van Dalen for valuable discussions.

[1]S. Pride, Phys. Rev. B **50**, 15678 (1994).
[2]S. R. Pride and M. W. Haartsen, J. Acoust. Soc. Am. **100**, 1301 (1996).
[3]M. W. Haartsen and S. R. Pride, J. Geophys. Res. **102**, 24745 (1997).
[4]S. S. Haines and S. R. Pride, Geophysics **71**, N57 (2006).
[5]S. Garambois and M. Dietrich, J. Geophys. Res. **107**, ESE 5 (2002).
[6]A. Jardani, A. Revil, E. Slob, and W. Söllner, Geophysics **75**, N19 (2010).
[7]A. Revil and A. Jardani, Geophys. J. Int. **180**, 781 (2010).
[8]D. Beamish, Geophys. J. Int. **137**, 231 (1999).
[9]G. I. Block and J. G. Harris, J. Geophys. Res. **111**, B01304 (2006).
[10]C. Bordes, L. Jouniaux, M. Dietrich, J.-P. Pozzi, and S. Garambois, Geophys. Res. Lett. **33**, L01302 (2006).
[11]K. E. Butler, R. D. Russell, A. W. Kepic, and M. Maxwell, Geophysics **61**, 1769 (1996).
[12]J. C. Dupuis, K. E. Butler, and A. W. Kepic, Geophysics **72**, A81 (2007).
[13]J. C. Dupuis, K. E. Butler, A. W. Kepic, and B. D. Harris, J. Geophys. Res. **114**, B10306 (2009).
[14]S. Garambois and M. Dietrich, Geophysics **66**, 1417 (2001).
[15]S. S. Haines, S. R. Pride, S. L. Klemperer, and B. Biondi, Geophysics **72**, G9 (2007).
[16]L. T. Long, W. K. Rivers, Geophysics **40**, 233 (1975).
[17]O. V. Mikhailov, M. W. Haartsen, and M. N. Toksöz, Geophysics **62**, 97 (1997).
[18]A. H. Thompson and G. A. Gist, The Leading Edge **12**, 1169 (1993).
[19]Z. Zhu, M. W. Haartsen, and M. N. Toksöz, Geophysics **64**, 1349 (1999).
[20]Z. Zhu, M. W. Haartsen, and M. N. Toksöz, J. Geophys. Res. **105**, 28055 (2000).
[21]Z. Zhu, and M. N. Toksöz, Geophysics **68**, 1519 (2003).
[22]D. E. Hall, *Basic Acoustics* (Wiley, New York, 1987).
[23]K. Aki, and P. G. Richards, *Quantitative Seismology* (University Science, Sausalito, CA, 2002).
[24]L. M. Brekhovskikh, *Waves in Layered Media* (Academic, New York, 1960).
[25]M. Schakel, and D. Smeulders, J. Acoust. Soc. Am. **127**, 13 (2010).
[26]D. L. Johnson, and T. J. Plona, J. Acoust. Soc. Am. **72**, 556 (1982).
[27]*CRC Handbook of Chemistry and Physics*, 90th ed., edited by D. R. Lide (Internet Version 2010). CRC Press/Taylor and Francis. http://www.hbcpnetbase.com/(2010).
[28]D. L. Johnson, J. Koplik, and R. Dashen, J. Fluid Mech. **176**, 379 (1987).
[29]D. L. Johnson, D. L. Hemmick, and H. Kojima, J. Appl. Phys. **76**, 104 (1994).
[30]J. Jocker, and D. Smeulders, Ultrasonics **49**, 319 (2009).
[31]C. J. Wisse, Ph.D. thesis, Delft University of Technology, 1999.
[32]S. R. Pride and S. Garambois, J. Eng. Mech. **131**, 898 (2005).